Advanced Materials

ADVANCED MATERIALS
www.advmat.de

RESEARCH ARTICLE OPEN ACCESS

Correlated Charge Transport in an Organic Coulomb Glass

Magdalena Sophie Dörfler[1] | Heinz Bässler[2] | Harald Oberhofer[3] | Anna Köhler[1,2]

[1]Soft Matter Optoelectronics and Bayerisches Polymerinstitut (BPI), Experimental physics II, University of Bayreuth, Bayreuth, Germany | [2]Bayreuth Institute of Macromolecular Research (BIMF), University of Bayreuth, Bayreuth, Germany | [3]Chair For Theoretical Physics VII and Bavarian Center for Battery Technologies, University of Bayreuth, Bayreuth, Germany

Correspondence: Anna Köhler (anna.koehler@uni-bayreuth.de)

Received: 18 November 2025 | **Revised:** 19 January 2026 | **Accepted:** 11 March 2026

Keywords: collective phenomena | disordered media | hopping dynamics | many-body effects | percolative conduction

ABSTRACT

Advances in the development of organic field-effect transistors (OFETs), electrically gated organic semiconductors (EGOFETs), and organic electrochemical transistors (OECTs) allow for the operation of these devices at very high charge-carrier densities, where Coulomb interactions between carriers can be expected to become significant. We have studied the effects of such Coulomb interactions in an OFET-like structure using Kinetic Monte Carlo (KMC) simulations. Compared to an analogous structure where carrier-carrier interactions are neglected, we find a reduction in carrier mobility and an increase in activation energy. This effect increases with increasing gate voltage, i.e., charge density. We associate this with the emergence of a different transport regime where correlated transport prevails and where a Coulomb gap appears in a dynamic density of states (DOS), consistent with previous work. We demonstrate that at these high densities, the charges in the organic semiconductor behave like those in a Coulomb glass. In this context, the activation energy for transport is reinterpreted to relate to the structural reorganization of the carrier ensemble. Unlike in inorganic semiconductors, for the organic semiconductor system, we find the appearance of a Coulomb gap to occur even at ambient temperature, and it does not require variable-range hopping.

1 | Introduction

The performance of organic electronic devices ultimately depends on the charge transport properties on the molecular scale. In organic field-effect transistors (OFETs), a higher charge carrier mobility decreases switching times and enables high-frequency operation [1]. In organic light-emitting diodes and organic solar cells, it leads to improved charge transport and reduces recombination losses [2, 3] while in sensors, a higher mobility results in better sensitivity and response time [4].

The mobility of charge carriers depends on their concentration. In systems with moderately high carrier density, such as OFETs, the mobility usually increases with carrier concentration. This is because the charges fill up the density of states (DOS) starting from the low-energy states, thereby raising the Fermi level. Thermally activated jumps of carriers from the Fermi level to the level where transport occurs efficiently (transport level) thus become increasingly easier with increasing concentration. However, at very high charge carrier concentrations, the carrier mobility has been observed to decrease with increasing concentration, which has been attributed to Coulomb repulsion between charges. Carrier concentrations at which this effect occurs can be achieved, for example, in OFET structures [5–9]. There, the high charge carrier density is achieved by increasing the gate voltage, on which the charge concentration depends linearly [10]. Fratini et al., for instance, observed current density saturation at high gate voltages in OFETs, which implies a decrease in mobility and a concomitant increase in activation energy at high concentrations [11]. They attribute both observations to Coulomb interactions between Fröhlich-polarons that form near the dielectric interface. However, there is still debate whether this

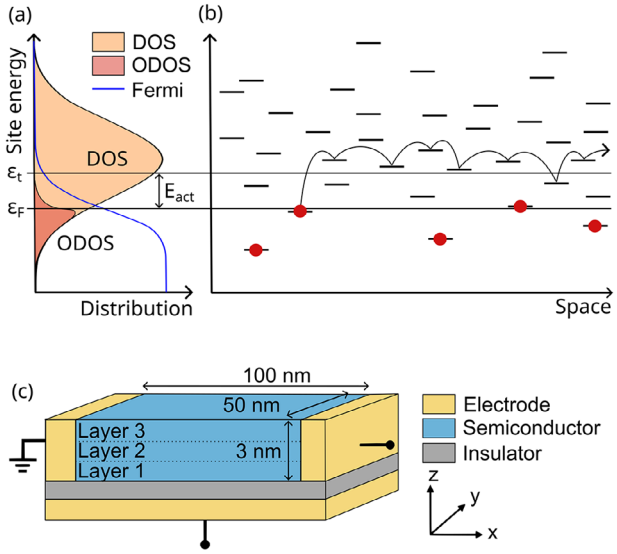

FIGURE 1 | Schematic illustrating the system modelled. (a) The distribution of the sites at different energies that are available for charges (DOS) and that are actually occupied by charges (ODOS). The Fermi-Dirac distribution is shown as a blue solid line, and the Fermi energy ε_F and the transport energy ε_t are indicated. (b) The distribution of available and occupied sites versus space. Dotted lines indicate ε_F and ε_t for reference, and a possible transport path for one carrier is shown. (c) The model geometry used in all simulations has periodic boundaries in the x- and y-directions.

is exclusively due to Coulomb interactions or whether extrinsic effects could also play a role [12, 13]. Simulations support that indeed Coulomb interactions are the main cause of the decrease in mobility at high concentrations [14–18]. These high charge concentrations can also be achieved in electrochemically doped systems [15, 19–23]. Recently, in an electrochemically doped tandem transistor structure at low temperatures (160K) and high charge concentrations, the gate-voltage dependence of the conductivity has been reported to exhibit an unusual behavior that may be associated with the appearance of a Coulomb gap [22, 23]. This soft gap in the density of states of the Fermi level was first described by Efros and Shklovskii [24] in disordered systems with strong localization and long-range Coulomb interaction between the charges, in particular, electron liquids at low temperatures. In these systems, a percolative, glassy transport behavior (Coulomb glass) can be observed, which is controlled by correlations [25]. Several theoretical studies and simulations of *inorganic* Coulomb glass systems have shown that Coulomb interactions ultimately lead to the formation of a Coulomb gap [24, 26–32]. Likewise, in simulations of *organic* semiconductors, Liu et al., Koopmans et al., and Ihnatsenka have shown the emergence of a Coulomb gap at uniformly high charge carrier concentrations [15, 33] or at interfaces where charge carriers accumulate [34].

However, a framework is still missing that explains how Coulomb gap formation leads to the observed decrease of mobility and the increase of the activation energy, and its impact on charge transport in organic materials, especially in OFETs, where high charge concentrations may be reached. To understand experimental observations and to study such fundamental concepts as charge transport, one needs to break down the complexity of a real system and use a simple model system, which is possible when using simulations. Extrinsic effects, such as altered injection or morphological changes, can be eliminated in simulations, allowing us to examine a disordered semiconductor's intrinsic behavior.

This paper shows whether and under what conditions a Coulomb gap forms in OFETs. To exclude effects due to counter-charges, we consider only non-doped systems. Electrochemical doping would add its own Coulomb effects and add a further level of complexity. This is why, in this work, we focus on the simplest case, i.e., without dopants. We link the emergence of a Coulomb gap to a change in the transport behavior where single charge transport evolves into correlated multi-charge transport, where a conventional description of charge transport does not hold. We propose a new interpretation of the role of the activation energy in the correlated transport regime and support this by a correlation analysis of charge transfer events. In this framework, we account for the experimentally observed mobility [5–9, 11] and activation energy [11]. Hence, our Kinetic Monte Carlo (KMC) simulations extend the conventional transport-level picture with a reinterpretation of the activation energy in the high charge concentration regime where correlated transport prevails.

2 | Concepts and Results

2.1 | Concepts

In disordered organic semiconductors, charge transport predominantly occurs via thermally activated hopping between localized sites, which can be, e.g., entire molecules or parts of a polymer chain. The energies of these sites form the density of states (DOS). These energies are usually spatially correlated [35, 36] and follow a Gaussian distribution ρ_{DOS} with a standard deviation σ [37, 38], which is known as the disorder parameter.

$$\rho_{DOS}(\varepsilon) = \frac{1}{\sqrt{2\pi}\,\sigma} \exp\left(-\frac{\varepsilon^2}{2\sigma^2}\right) \tag{1}$$

In an equilibrated system, the Fermi-Dirac distribution

$$W_{Fermi}(\varepsilon) = \left(\exp\left(\frac{\varepsilon-\mu}{k_B T}\right)+1\right)^{-1} \tag{2}$$

describes the occupation probability of a particular energy level ε. It only depends on the temperature T and the chemical potential μ, which is the Fermi level ε_F at zero temperature. k_B is the Boltzmann constant. The density of all occupied states (ODOS), ρ_{ODOS}, is then the product of (1) with (2),

$$\rho_{ODOS}(\varepsilon) = \rho_{DOS}(\varepsilon) \cdot W_{Fermi}(\varepsilon) \tag{3}$$

and thus coincides with the low-energy tail of the DOS. Figure 1a illustrates the relation between the DOS, ODOS, and the Fermi function, and Figure 1b shows a typical associated path for charge transport. For low and moderate charge density, most charges (red dots) occupy sites at the Fermi level ε_F or below. Only a few (empty) sites are energetically and spatially sufficiently close to the sites occupied by charges to allow for charge transfer

events with a reasonable probability. Thermal activation with an activation energy E_{act}, however, can promote charges to a site closer to the centre of the DOS where there are enough empty neighboring sites to allow for hopping over several adjacent sites with a high probability before relaxing again to a site in the tail of the DOS. This significantly improves the transport of the charge carrier. The threshold energy at which this quasi-percolative charge transport sets in is known as the transport energy ε_t [39–41]. Since the hops from the low-energy sites to sites above ε_t are the rate-limiting steps in this transport mode, the activation energy for these hops can easily be determined by measuring the temperature-dependence of the mobility $\mu(T)$ and fitting an Arrhenius dependence, $\mu(T) \propto \exp(-E_{act}/k_BT)$, to it [41].

The traditional concept of hopping transport depicted in Figure 1a,b has been derived for the case of low and moderate charge density, where Coulomb interactions between charges can be neglected. We aim to explore how charge transport changes when the charge carrier density becomes sufficiently high for their mutual Coulomb interaction to become noticeable.

Our current study is based on Kinetic Monte Carlo (KMC) simulations. Figure 1c illustrates the studied geometry resembling an organic field-effect transistor (OFET). We simulate charge transport only within the semiconductor material, with periodic boundary conditions along the x- and y-axis. Figure 1c indicates the simulation box size along each axis; the lattice constant is $a = 1$ nm [38] in all directions. In the non-periodic z-direction, we use three layers, which is sufficient since most charges accumulate at the insulator interface [5, 18, 42]. Due to the insulator in the OFET, the gate electrode and the semiconductor can be approximated to form a capacitor, where the number of charge carriers N in the semiconductor linearly depends on the applied gate voltage V_G V [10]:

$$N = \frac{\varepsilon_{ins}\varepsilon_0 \times A \times V_G}{q \times d_{ins}} \tag{4}$$

Here, $\varepsilon_{ins} = 4$ and $d_{ins} = 100$ nm are the relative permittivity and thickness, respectively, $A = 5000$ nm^2 is the area of the insulator-semiconductor interface, ε_0 is the vacuum permittivity, and q is the unit charge. We take the number of charges as constant and initialize their positions randomly.

To calculate the single-charge-transfer probabilities, we apply the so-called "full" Miller-Abrahams (MA) rate given in Equation (5), instead of the commonly known and conventionally used version of the MA rate. The latter, with a constant term for hops downward in energy and a Boltzmann term for upward hops, is actually an approximated version that becomes inadequate in the limit of weak disorder or high electric fields as discussed in ref. [43, 44, 47]. This becomes relevant for systems considered in our study. Both rates consider the energy conservation for charge transfer by the emission or absorption of a single phonon [45], yet they differ in the assumptions made for the spectral phonon density [44, 46]. While the "full" rate assumes a linearly increasing phonon density with increasing energy, the conventional rate assumes a monotonic increasing, yet eventually saturating dependence that approaches a constant value. In any case, the energy gap between adjacent hopping sites must not exceed the energy of the phonons concerned [47], and the temperature needs to be sufficiently high for the relevant lattice vibrations to be excited [48]. Though the rate was originally derived for charge transfer in systems with low impurity concentrations [45], this was mainly to avoid the emergence of energy bands and does not concern the dependence on charge carrier concentration [45].

The full MA rate, describing a charge transfer from an occupied to an unoccupied site, reads as follows [43, 44]:

$$k_{ij} = \frac{C}{\hbar} e^{-2\gamma r_{ij}} 2k_BT \frac{\frac{|\varepsilon_j - \varepsilon_i|}{2k_BT}}{\sinh\left(\frac{|\varepsilon_j - \varepsilon_i|}{2k_BT}\right)} e^{-(\varepsilon_j - \varepsilon_i)/2k_BT} \tag{5}$$

Here, k_B is the Boltzmann constant, and T the system temperature. The maximal hopping distance r_{ij} is $\sqrt{3}a$, the dimensionless constant $C = 1$, and the inverse localisation radius $\gamma = 5$ nm^{-1} for all cases. The single-site energies (ε_i, ε_j) of the initial and final positions are computed by adding the respective correlated site energies, the potential caused by the electrical fields, and the potential due to Coulomb interactions with other charges. After calculating the rates for all possible transfer events, one event is randomly chosen according to its weighted probability and executed. The time elapsed for this event is $\delta t = -\ln(X)/k_{total}$, where $\boldsymbol{X}$ is a random uniform number $X \in [0, 1[$ and k_{total} is the sum of all rates [49]. After the jump is executed, the potential landscape is updated, avoiding the self-interaction error as described by Li and Brédas [50].

The static site energies are calculated by the dipole method described by van der Holst et al. [17] such that they follow a correlated Gaussian distribution. The electric field created by the gate electrode (source-drain electrode) is implemented by defining a linear potential gradient along the z-direction (x-direction). The Coulomb interactions between charge carriers are either intentionally neglected, to provide a reference system, or included in the potential landscape and calculated according to the *Minimum Image Convention* [51, 52], which leads to an effective cutoff radius of half the box length along the x- and y-axis. The dielectric permittivity of semiconductors is usually measured as an average value at low carrier density. Evidently, at high charge carrier density, the polarizability of a material may increase, and hence the dielectric screening might increase as well. This effect, as well as local deviations, is not considered in our approach, as we use a density-independent dielectric constant of $\varepsilon_r = 4$. We consider a simulation to have reached (quasi-)equilibrium when at least a minimum of $2 \cdot 10^7$ simulation steps have been performed, and the current density in the x-direction has converged, which is declared when the coefficient of variation falls below 5%. Depending on the number of charge carriers, we perform several simulations until the transport of a minimum of 100 charges has been simulated. For more details on the simulation approach, especially the implementation of the electrical fields, see Supporting Information (Section A).

2.2 | Mobility Decay at High Voltages

To assess the effect of including carrier-carrier interactions in the hopping transport, we simulated the charge transport in the OFET structure of Figure 1c with and without Coulomb

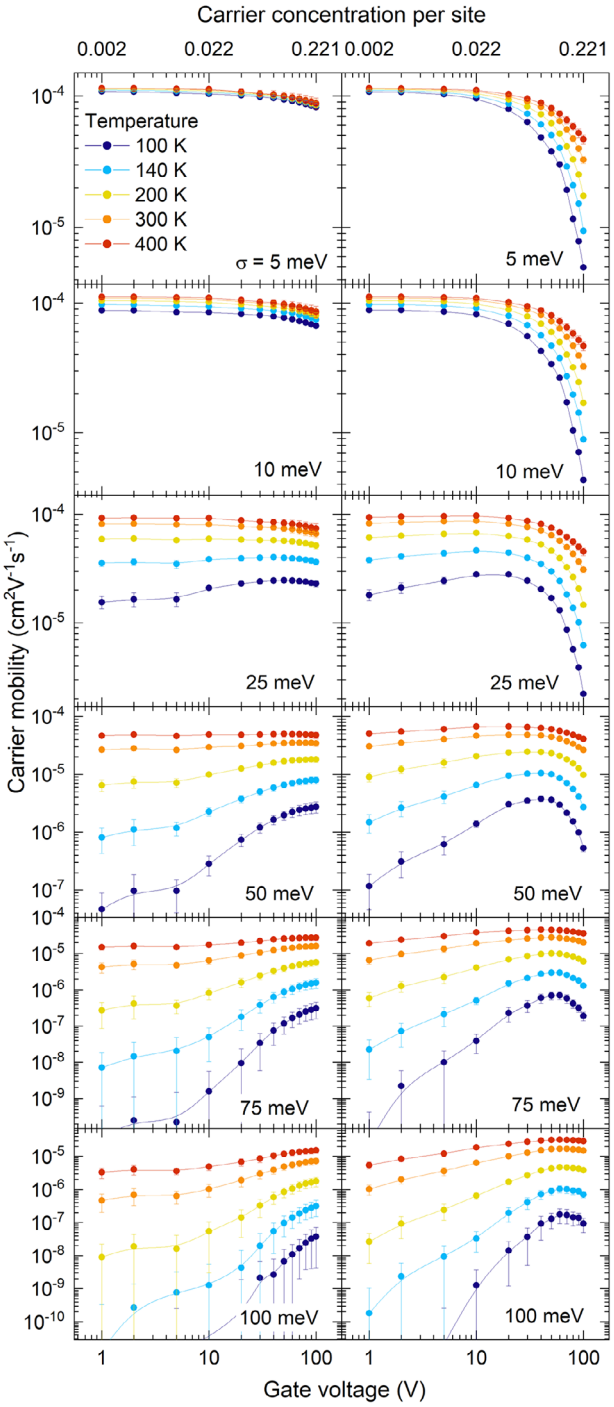

FIGURE 2 | Gate voltage dependence of the charge carrier mobility when Coulomb interactions between carriers are not included (left panel) or included (right panel) in the simulations, for different disorder strengths σ and temperatures T. When assuming that only the lowest layer is occupied, the top scale specifies the respective charge concentration per site in this layer.

interactions included in the simulations as a function of carrier density, i.e., parametric in the gate voltage. After equilibration of the simulations, we calculate the average charge carrier mobility $\mu = v/F$ from the carrier drift velocity v and the electrical field F for each carrier and take the standard deviation as a measure of the confidence intervals. Figure 2 compares the average charge carrier mobility obtained for different disorder strengths σ.

For low gate voltages and hence low carrier densities, the charge carrier mobility does not change significantly when carrier-carrier interactions are explicitly considered compared to the mobility without. In contrast, for higher gate voltages and concomitantly high carrier densities, including carrier-carrier interactions reduces the mobility. For qualitative comparison, the difference between the two mobilities is also plotted in Figure S1. The dependence of the mobility on gate voltage, i.e., carrier density, changes with disorder. For disorder strengths of 25 meV and weaker, the mobility decreases with gate voltage for both cases, with and without inclusion of carrier-carrier interactions, but in the absence of interactions, the effect is very small. With increasing disorder strength, one observes that the mobility increases with gate voltage, goes through a maximum, and then decreases at very high gate voltages. The maximum of the mobility shifts toward higher gate voltages with increasing disorder. We will come back to this later.

The comparison between the data set with and without inclusion of carrier-carrier interactions implies that the primary reason for the mobility decrease at high charge concentrations in OFETs is the interactions. This result is conceptually consistent with previous studies in 3D-periodic systems [14–16]. Note, however, that the gate field introduces a charge density gradient and, therefore, enhances the 2D nature of charge transport in OFETs [5, 42]. Minor quantitative differences in the extent of the decrease and the concentration at which it sets in can be attributed to differences in simulation parameters such as the dielectric constant or the delocalization radius, as discussed before [15, 16].

Although it is generally accepted that carrier-carrier interactions are the leading cause of mobility reduction, there are different explanations for how they affect charge transport. Zhou et al. suggested that at high concentrations, additional energy barriers created by carrier-carrier interactions hinder charge transport [14]. Liu et al. describe the transport as "to some extent similarly to a strongly correlated system ("Coulomb glass")" [16], which Koopmans et al. illustrate by showing that carrier-carrier interactions lead to the formation of a Coulomb gap in the DOS of organic semiconductors [15]. They suggest that the gap "reduces the number of available hopping sites in the vicinity of the Fermi level" [15], forcing the charges to hop to either higher-energy sites or over larger distances, both leading to a decreased mobility. In order to understand the formation and nature of this Coulomb gap, we first consider the DOS and ODOS obtained from the simulations of the data shown in Figure 2.

2.3 | Coulomb Gap Evolution and Broadening of the DOS

We obtain the ODOS and DOS from histograms over the resulting site energies, where we considered 50 different configurations after equilibration, read out after 10^4 hopping events each time. We obtain the Fermi function and the corresponding Fermi level by fitting Equation (2) to ρ_{ODOS}/ρ_{DOS} at a fixed ambient temperature. The evolution of the DOS and ODOS with increasing gate voltage and hence increasing charge density for the cases with and without consideration of carrier-carrier interactions is

shown in Figure 3, at a temperature of 300 K. The system behaves very similarly at all temperatures studied; for reference, we show the respective data for 100 K in Figure S2. We focus on the two examples where the energetic disorder in the sample prior to applying a gate voltage is either very low (5 meV) or moderately high (75 meV). When a gate voltage is applied, the associated charges and their Coulomb interactions increase the absolute value of the potential energy. We decided to shift all distributions so that the DOS considered is always centered around zero energy. This representation allows for a better comparison and, at the same time, does not complicate further discussions, since only relative energy differences are relevant for charge transport.

Let us first consider the case of small disorder (Figure 3a) without carrier-carrier interactions. For $V_G = 1$ V, the DOS is a very narrow Gaussian with $\sigma = 5$ meV. All three layers of the simulated OFET (c.f. Figure 1c) contribute equally to this Gaussian. At higher gate voltages, the DOS evolves into three Gaussians of lower height yet with the same standard deviation; every layer contributes to one peak. The gate field is responsible for this splitting, which increases linearly with gate voltage: The field in the z-direction lowers the potential equidistantly for each layer, dependent on the distance of the layer to the insulator. As expected in an equilibrated system, we find the ODOS at low energies, i.e., in the first layer. Within this first layer, the ODOS is nearly evenly distributed because the DOS is narrower than the available thermal energy (see Figure S3).

Now we turn to the case with Coulomb interactions between carriers. Even at the lowest charge density (approximately 0.07% of the sites) of $V_G = 1$ V, there is a remarkable difference to the case without interactions: The DOS is asymmetric, and each layer's peak is significantly broadened. Upon increasing the gate voltages, the gate field splits the DOS again into different peaks for the different layers; however, the splitting is no longer equidistant. Rather, it decreases drastically at higher energies, so that the DOS of the second and third layers largely overlap. Similarly, the DOS is broader in the lower layer. Furthermore, the explicit inclusion of carrier-carrier interaction has caused the DOS width of the first layer at 100 V to increase from $\sigma = 5$ meV to approximately $\sigma = 110$ meV. A similar increase in DOS width applies to other disorders (see Figure S4), though the Coulomb-induced broadening reduces when the already prevailing energetic disorder increases. From the ODOS, we see that most charges occupy the low-energy sites in the first layer, next to the gate insulator. We therefore attribute both the decreased splitting and the reduced width of the DOS in the higher layers to the effect that the Coulomb potential generated by the charges in the first layer screens most of the gate-induced potential.

The main difference, however, between the case without and with consideration of Coulomb interaction between carriers is the emergence of a fourth peak: At 20 V, it is visible as a low-energy shoulder of the first layer's DOS, and above 60 V, it is recognizable as a distinct peak. It becomes higher, more expressed, and shifts toward lower energies as the gate voltage increases. It is particularly noteworthy that the ODOS of the entire OFET coincides with this additional peak in the DOS of the first layer, though it does not fill it entirely (c.f. Figure S5). The gap that therefore emerges between the unoccupied and occupied sites in the first layer's DOS is the Coulomb gap. It was first described by Efros and Shlovskii for an inorganic Coulomb glass [24, 32] and also observed in organic semiconductor simulations by Koopmans et al. for the 3D charge transport case without gate voltage [15]. We will discuss its existence and shape further below and in the Supporting Information (Section D).

Figure 3b shows similar data, only at a higher disorder strength of 75 meV. Analogous to the 5 meV case, we observe the appearance of a Coulomb gap and a reduced energetic offset for the second and third layers' DOS parts. There is, however, one difference compared to the example with $\sigma = 5$ meV disorder. For $\sigma = 75$ meV, the DOS part of each layer is already broad. Therefore, the additional broadening induced by carrier-carrier interactions is not as pronounced (see also Figure S4).

In Figure 3c,d, we compare cases at opposite ends of the explored disorder and temperature ranges at $V_G = 100$ V. Evidently, the Coulomb gap is present at all disorders; only the additional broadening due to Coulomb interactions becomes less prominent when the DOS is already broad due to energetic disorder. At 100 K, the DOS is slightly less broadened and reduces to zero at the center of the Coulomb gap. At higher temperatures, the gap becomes slightly softer but is still well pronounced. This can also be seen in Figure S2, where we show the same data as in Figure 3a,b at 100 K.

2.4 | Arrhenius Dependence and Activation Energy

Having derived the form of the DOS from the KMC simulation, we shall assess its impact on the charge transport. For this, we first investigate the influence of temperature on charge transport. We extract the activation energy for different disorders and gate voltages by fitting an Arrhenius dependence, $\mu(T) = \mu_0 \exp(-E_{act}/k_B T)$, to the temperature-dependent mobility. Figure 4 (a) shows examples for $\sigma = 5$ meV and 75 meV at different gate voltages, with the Arrhenius fits as lines to the data points.

Let us first consider the influence of carrier density on the mobility when carrier-carrier interactions are neglected (left panels of Figures 2 and 4a). For a disorder of $\sigma = 75$ meV, increasing the gate voltage (and hence the carrier density) increases the absolute value of the mobility and the slopes of $\mu(T)$ become shallower, i.e., the activation energy reduces. This phenomenon is well-understood. With increasing carrier density, the Fermi level ε_F rises and moves closer to the transport level ε_t (cf. Figure 1), hence less activation energy is required for a concomitantly faster transport. For very low disorders such as $\sigma = 5$ meV, the curves barely show any slope and do not change with gate voltage, except for the absolute value, which reduces. We consider that this reduction arises because for the nearly disorder-free case at $\sigma = 5$ meV, the Fermilevel and the transport level are already very close. Hence, increasing the gate voltage does not change the required activation energy. However, at high carrier densities, partial occupation of available sites can block some of the carrier jumps in field direction, notably in a quasi-2D system, and thus slightly reduce the absolute value of the mobility.

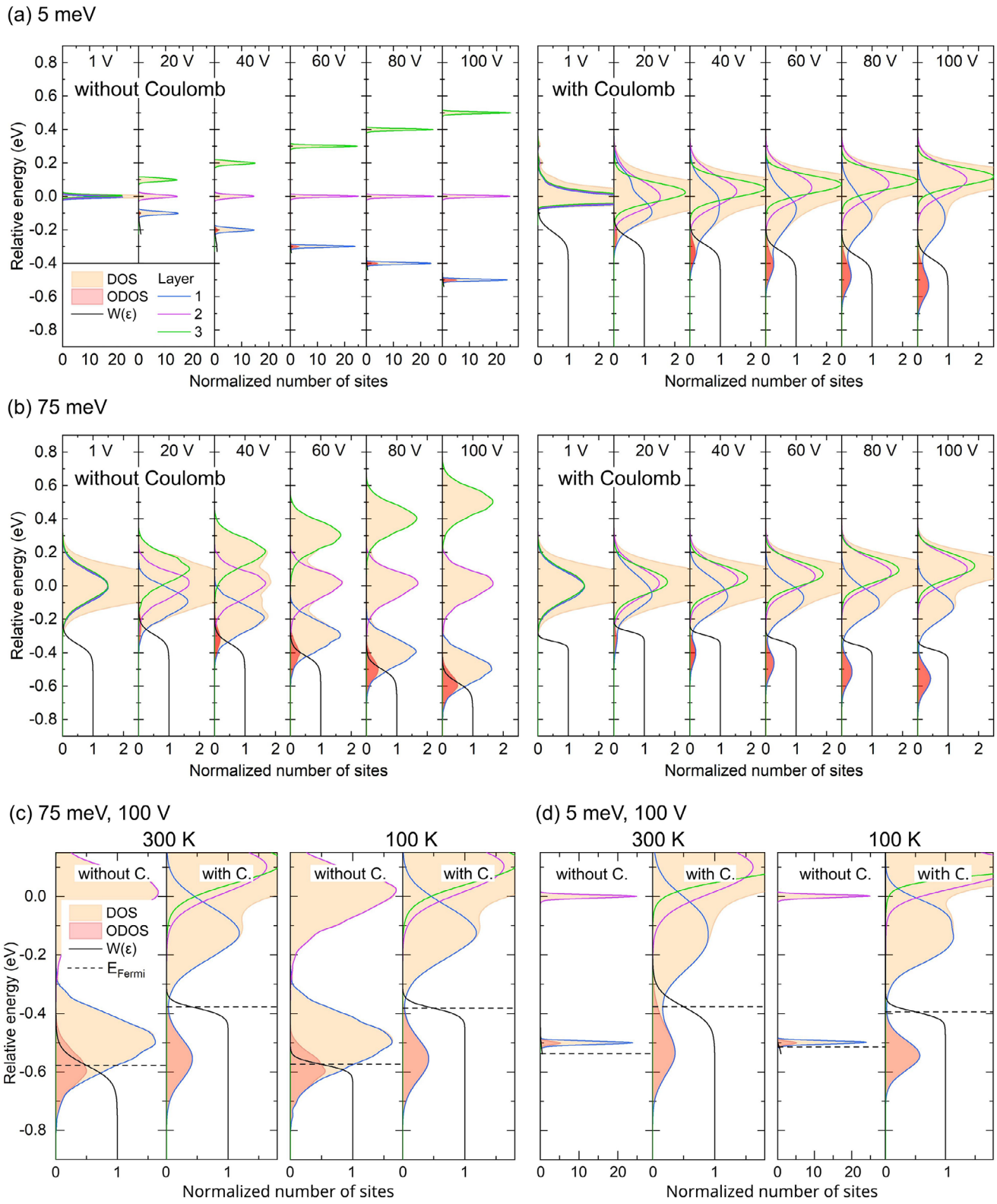

FIGURE 3 | The evolution of DOS (light orange) with increasing gate voltage for simulations with and without carrier-carrier interactions for a disorder strength of (a) 5 meV and (b) 75 meV at 300 K. For display purposes, the DOS is centered around zero energy. The blue, purple, and green lines indicate the contribution to the DOS from the sites in different layers of the simulated OFET. The ODOS (red) and the Fermi distribution (black line) are also shown. (c,d) Comparison of the DOS for simulations with and without carrier-carrier interactions for representative cases of low and high disorder ($\sigma = 5$ meV, 75 meV) and low and high temperatures ($T = 100$ K, 300 K) at $V_G = 100$ V.

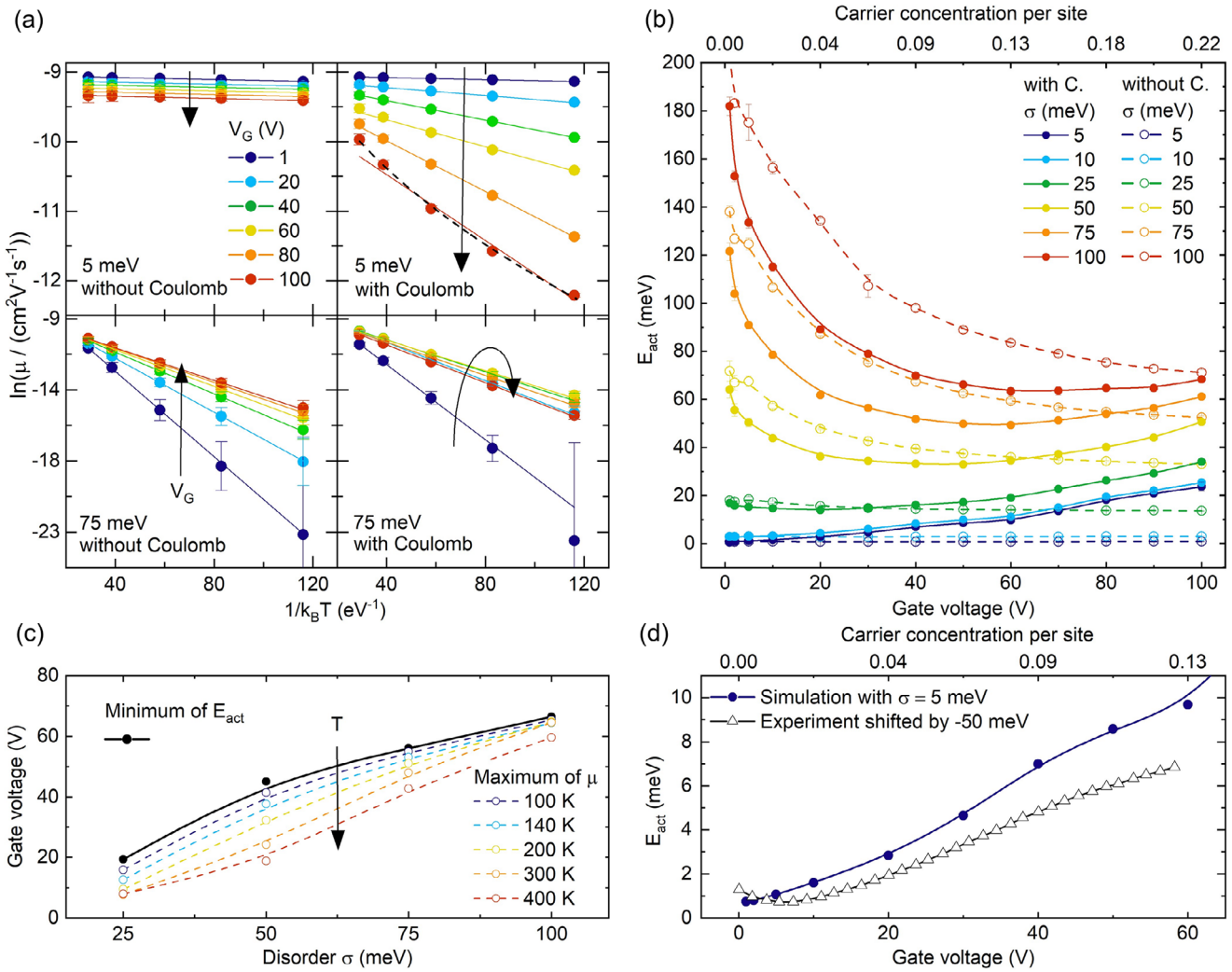

FIGURE 4 | (a) Arrhenius fits (solid lines) to the mobility obtained for different gate voltages without (left panels) and with (right panels) carrier-carrier interactions. The top and bottom panels exemplify the data for $\sigma = 5$ meV and 75 meV, respectively. Black arrows indicate the increasing gate voltage parameter. An Efros-Shklovskii fit with $T_0 = 2012$ K to the curve for $\sigma = 5$ meV, $V_G = 100$ V, with carrier-carrier interactions is additionally displayed (black dashed line). (b) The dependence of the activation energy on the gate voltage with (solid lines) and without carrier-carrier interactions considered (dashed lines) for different disorder strengths σ. Note that the curves for $\sigma = 5$ meV and 10 meV superimpose for the case without interactions. (c) Gate voltage of the minimum activation energy compared to the gate voltage of the maximum mobility for different temperatures versus disorder strength (lines are guides to the eye). (d) Comparison of the simulation results for $\sigma = 5$meV to the experimental data from Fratini et al. [11], which are shifted about −50 meV.

This picture changes when carrier-carrier interactions are included so that the combined effects of electron repulsions and the concomitantly increasingly broadened DOS become noticeable (right panels of Figures 2 and 4a). For the $\sigma = 5$meV case, the temperature dependence, and hence E_{act}, gets stronger with increasing gate voltages. Moreover, the temperature dependence of the mobility begins to deviate from a simple Arrhenius dependence. For a gate voltage of 100 V, the temperature dependence of the mobility finally approaches a $\mu(T) \propto \exp\left(-(T_0/T)^{\frac{1}{2}}\right)$ law which Efros and Shklovskii consider as a signature for the formation of a Coulomb gap [24]. It implies that under these conditions, charge transport is temperature-activated, yet the activation energy decreases with decreasing temperature. An Arrhenius-type fit can therefore only approximate the change in activation energy with increasing charge concentration. For the case of higher disorder, σ = 75 meV, the slopes first decrease with gate voltage up to V_G = 60 V and then increase again. We consider that two effects superimpose. For gate voltages below 60 V, the effect of filling up of the DOS dominates, hence the activation energy reduces with increasing gate voltage. At higher voltages, carrier-carrier repulsions and the (slight) Coulomb-induced broadening of the DOS lead to an increase in thermal activation for $\mu(T)$.

Figure 4b compares the dependence of the activation energy on the gate voltage with and without carrier-carrier Coulomb interactions for different disorder strengths. When displayed as a direct comparison, one can clearly observe that for low disorders, such as below 25 meV, carrier-carrier interactions change a previously virtually gate-voltage independent, nearly non-activated transport process into one that requires nearly linearly

increasing thermal activation energy as the gate voltage increases. For disorders above 25 meV, the activation energy decreases monotonously with gate voltage if carrier-carrier interactions are neglected. Including carrier-carrier interaction reduces the activation energy for lower gate voltages until E_{act} increases again and finally exceeds the interaction-free value. It is remarkable that in a disordered system, an even moderate concentration of charges (at $V_G = 10$ V, no more than about 1% sites are occupied) can decrease E_{act}. It demonstrates that the presence of the long-range Coulomb interactions can smooth the energetic landscape quite before carrier-carrier repulsion sets in at a higher gate voltage [14]. In the following, our focus will be on the minimum in the gate-voltage dependence, and in particular on the increase in activation energy for higher gate voltages. Evaluating the gate-voltage dependence of the activation energy for all temperatures studied shows that for 100 K, the minimum in the gate-voltage dependence of E_{act} coincides with the maximum in the gate-voltage dependence of $\mu(T)$ (see Figure 4c). Evidently, this gate voltage marks the transition to the regime where carrier-carrier interactions dominate the transport behavior. If one likes to define a range beyond which Coulomb glass behavior becomes dominant, then the minimum of the activation energy would give a suitable value, as this is the charge carrier density where the effect of a Coulomb gap on transport dominates over those due to intrinsic disorder. Its dependence on gate voltage translates linearly into a charge carrier density dependence, with 10 V corresponding to a density of $2.2 \cdot 10^{12}$ cm^{-2} or 2.2%, provided that all carriers are assumed to be in the bottom layer.

It is very satisfying that our KMC-based results agree with the experimental findings of Fratini et al., who also observe an increase in the activation energy at very high charge density in single-crystal rubrene OFETs [11]. They also attribute this to the importance of carrier-carrier interactions, although they include interactions of Fröhlich polarons in the analysis of their data instead of bare charge carriers. Figure 4d compares our findings to their experimental results shifted by −50 meV. As can be seen, the trend in activation energy corresponds well. The quantitative difference, notably the offset for small V_G, arises mainly because we simulate a disordered system without consideration of polaronic contributions. In contrast, Fratini et al. studied a highly ordered system with a highly polarizable dielectric. Therefore, they derive the activation energies by analyzing the experimental data in a polaronic framework [53]. The salient feature, however, is the agreement in the increasing activation energy with increasing carrier density in our simulations and in their experimentally derived data. Importantly, this can be attributed to the Coulomb interaction between the charges in both cases. Further minor differences result from our choice of simulation parameters, such as the dielectric constant and lattice properties, compared to the properties of rubrene crystals.

2.5 | Activated Transport with a Coulomb Gap

In the following, we want to illuminate why the activation energy shows the trend just discussed and what this means for transport behavior. We will demonstrate that with increasing charge carrier concentration, a transition from single-carrier transport to correlated, quasi-collective transport behavior takes place. Due to the discrete nature of the KMC simulation, no instantaneous reorganization of the other carriers can occur. Rather, reorganization takes place through subsequent hops of adjacent carriers. In this picture, it is no longer sufficient to consider activation energy as the energy required to raise a single charge carrier to the transport level in a static DOS. Instead, activation energy is the energy required to enable the entire ensemble to move within a dynamic DOS. To start, we analyze the nearly-disorder-free case of $\sigma = 5$ meV in more detail. Figure 5 shows a zoom-in of the DOS and ODOS in the region around the Coulomb gap for $\sigma = 5$ meV, $T = 100$ K, for different gate voltages. Let us consider first the data for $V_G = 20$ V. The explicit inclusion of Coulomb interactions between carriers caused a significant broadening of the DOS and a low-energy shoulder that is almost entirely filled, thus forming the ODOS. The Fermi level ε_F is defined by the Fermi-Dirac distribution as the energy at which the probability to find an electron is exactly 50%. We show it as a black dashed line.

In the classical, one-particle transport picture, which we introduced at the beginning of this section (c.f. Figure 1) and that neglects carrier-carrier interactions, charge transport is enabled by thermally activated hops of carriers from the Fermi level to the transport level, which is somewhat below the center of the DOS [39]. Figure 5 shows, however, that the Fermi level is always located in the middle of the Coulomb gap, where the DOS is minimal. Conventionally, thermal activation with E_{act} should raise a carrier from the Fermi level to the transport level. However, the energy $\varepsilon_F + E_{act}$ is, first, far away from the center of the DOS and, second, and concomitantly, at an energy where the number of available sites has not changed significantly. Hence, the notion of "conventional" transport, where the carrier hops thermally activated to a site where subsequent efficient quasi-resonant transport occurs, does not hold. One might argue that this is nevertheless consistent with the decrease in mobility in the presence of the Coulomb gap. However, it raises the question of why the activation energy is not significantly larger, allowing charges to overcome the width of the Coulomb gap, where the DOS is minimal, and find more available sites in the free DOS. The thermal energy available at 100 K is about 8.6 meV, yet the activation energy for $V_G = 20$ V and $\sigma = 5$ meV is only 2.8 meV.

To understand this, we examined the characteristics of single-hopping events. We obtained the mean initial energy at which hopping occurs by averaging over the initial energies of 500 consecutive hopping events in the ensemble (from different carriers) that were executed after equilibration. To our surprise, we found that the mean initial energy (red dashed line) before a hop takes place is not the Fermi level – quite to the contrary, it is at much lower energies at the center of the ODOS. If we add the observed activation energy to the mean initial energy, we obtain a value that still lies close to the center of the ODOS (red dotted line). The fact that the average energy of hopping charges is close to the center of the ODOS implies that all charges contribute to transport, not only the ones at the Fermi level. We will demonstrate and discuss this in the following.

This finding seems puzzling at first sight, since hops to already occupied sites are not allowed (by simulation constraints). Moreover, in the center of the ODOS, i.e., away from the Fermi level,

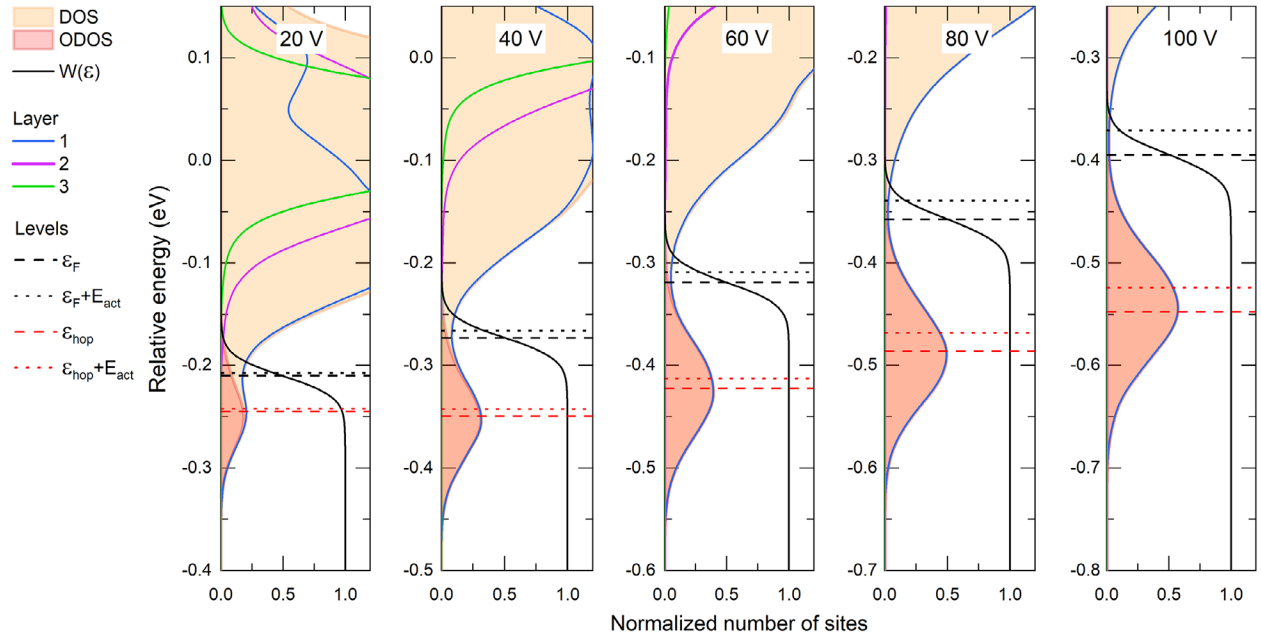

FIGURE 5 | Energy levels in the DOS (light orange) for 5 meV disorder at 100 K, for different gate voltages in each panel. The ODOS is light red, and the Fermi function (black solid line) indicates the fraction of occupied states. The Fermi level energy level ε_F is shown as a black dashed line, and the classical transport level $\varepsilon_F + E_{act}$ as a black dotted line. The initial energy of an average hopping event ε_{hop} is indicated by a red dashed line, while the level $\varepsilon_{hop} + E_{act}$ is shown as a red dotted line.

the DOS seems fully occupied. However, close inspection shows that at the energy corresponding to the center of the ODOS, there is still a small, albeit finite number of unoccupied sites (see Figure S5). More importantly, when including Coulomb interactions between carriers, the DOS and ODOS acquire a dynamic, multi-particle character. The classic transport picture that we described above, without explicit consideration of carrier-carrier interactions, is based on a single-particle picture, where the hop of one carrier proceeds in a static DOS and ODOS. The presence or absence of this carrier is not considered to affect the energy of other sites in the DOS or ODOS. The explicit inclusion of carrier-carrier interactions implies that the multi-particle nature of this interaction has to be considered, because the presence of one carrier alters the energies of all other occupied or unoccupied sites by virtue of its associated long-range Coulomb potential. Notably, the site energies in the local environment of the considered charge carrier may differ significantly from the globally averaged site energies expressed in the mean DOS and ODOS. In Figure 6, we shall take a closer look at this.

Figure 6a shows the site energies in the conventional single-particle picture, neglecting carrier-carrier interactions. Sites are subject to some degree of statistical energetic disorder. A charge (light red) will occupy a site at low energy without affecting the site energy itself, nor the energy of other empty or occupied sites nearby. The DOS simply results from summing up all site energies, leading to a Gaussian distribution. Figure 6b illustrates the situation when carrier-carrier interactions are explicitly considered. With Coulomb repulsion, charges will predominantly arrange themselves so that the distances to their neighbors are as large as possible. Hence, a particular carrier that is considered sits at the minimum of its potential. Unoccupied sites further away from the considered carrier are, necessarily, closer to other charges and therefore at higher potential energy. The red line indicates this distance dependence in the resulting site energies. Importantly, the same consideration applies to any other carrier considered at any other site. Averaging over the entire ensemble – under consideration of these multi-particle aspects – results in the binomial DOS depicted, with the soft gap separating the unoccupied sites from the occupied ones.

To probe this picture, we read out the energies at and near a site of a particular carrier immediately before it hopped. We did this for the 500 consecutive hopping events we examined earlier, and for different gate voltages, at $\sigma = 5$ meV and $T = 100$ K. We take the energy relative to the site energy at the initial carrier position and average over all configurations. Figure 6c depicts the site energy versus the distance from the initial position of the considered carrier in the hopping direction, ultimately, before it hops. Figure 6d shows a zoom-in on the data from Figure 6a. Because the lattice unit of the simulation box is $a = 1$ nm, this is also the resolution of the potential.

We indeed find that the site energies have a minimum around the carrier we considered, for all gate voltages, and as the distance from its initial position increases, the site energy increases to reach an approximately constant value at large distances. This confirms the conceptual picture of Figure 6b. With increasing gate voltages, the local minimum in the site energies becomes narrower and deeper. With increasing gate voltage and thus for a higher charge carrier density, the distances between the charge carriers become smaller. The site energy, therefore, increases more rapidly with increasing distance. Additionally, more charges contribute to the mutual repulsion, and, therefore, the site energies at large distances from the considered carrier are higher.

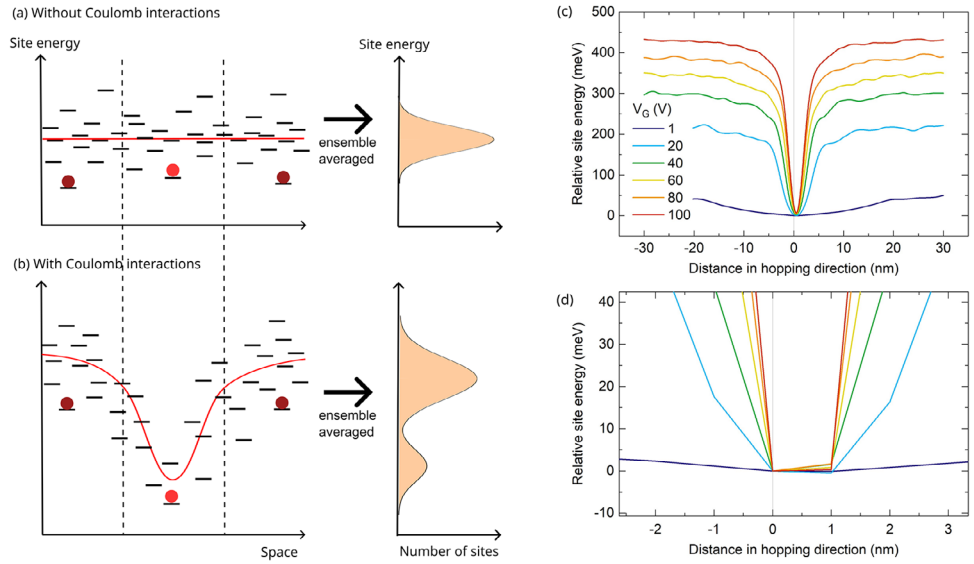

FIGURE 6 | (a,b) Illustration of site energies a single carrier (light red) experiences in the presence of other charges (dark red). The left part indicates the distribution of the sites in space, while the right part shows the DOS that results when averaging over the entire ensemble of carriers. Carrier-carrier interactions are neglected in (a) and included in (b). A red line illustrates the average site energy distribution in the space surrounding the considered carrier. (c) The average initial potential a charge experiences before it hops. The potential is plotted against the positive hopping direction and shown for several gate voltages at $\sigma = 5$ meV and $T = 100$ K. (d) Enlarged version of (c).

The zoom-in in Figure 6d shows that, on average, the energy landscape around a charge carrier immediately prior to its jump is not perfectly centered around the site on which the carrier is located. Rather, it is slightly tilted in the positive hopping direction. This energy landscape results from the Coulomb interaction of the considered carrier with all other carriers in the vicinity (cf. Figure S7). Evidently, the overall carrier arrangement must have been in such a way that the considered carrier is no longer in the center of the potential valley. Rather, this center, where the potential energy is minimal, lies in the direction of the jump, implying that the carrier can jump "in fair weather" [30]. The jump of the carrier is therefore caused by the change of the energy landscape surrounding it, and it is a direct reaction to the movement of the other carriers. Thus, the transport is evidently correlation-controlled.

Figure 6d also gives rise to a question. If the jump – on average—occurs in the direction of an energy minimum, it requires no or only small energy, much less than the activation energy shown in Figure 4. Why then is the mobility thermally activated (c.f. Figures 2 and 4)? To understand this, we emphasize that Figure 6d delineates the average site energies in the hopping direction. There are, however, also many jumps that occur energetically uphill and thus require activation energy. This is shown in Figure 7. Downhill jumps do not require activation energy, while uphill jumps do. If we calculate the average positive energy barrier for the gate voltages from 1 V to 100 V, we find values of 5 meV, 10 meV, 15 meV, 16 meV, 20 meV, and 18 meV, respectively.

Our central argument regarding the carrier transport in the regime of high carrier densities will be that the hops of different carriers are correlated. The jump of one carrier induces the jump of another by virtue of their Coulomb interaction, so that the ensemble of carriers moves as a whole. From time to time, a carrier may be surrounded by energetically uphill sites and will only be able to hop further if provided with some activation energy. It is this activated jump that is rate-limiting for the motion of the entire ensemble [31].

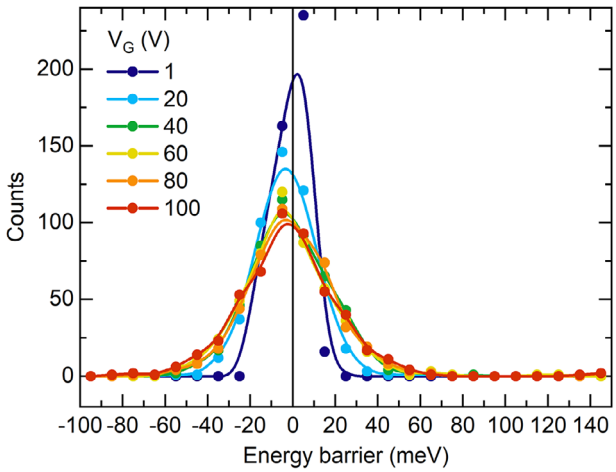

FIGURE 7 | The distribution of energy barriers in hopping direction for different gate voltages V_G for $T = 100$ K and $\sigma = 5$ meV. The energy barrier is the difference between the energy at a 1 nm hopping distance and the energy at the initial position of the hopping charge carrier for 500 consecutive events. The bin size was 10 meV.

2.6 | Correlation-Controlled Transport

To study the correlation between individual jumps, we use the velocity cross-correlation function (VCCF).

$$C_{ij}(r,\tau) = \left\langle \frac{1}{N(r,t)} \sum_{|\boldsymbol{r}|=r} v_i(\boldsymbol{x},t) \cdot v_j(\boldsymbol{x}+\boldsymbol{r}, t+\tau) \right\rangle_t \quad (6)$$

It computes the correlation between the velocity components v_i, v_j in a certain direction ($i,\ j \in [x, y]$) for all the positions $\boldsymbol{x}$ and $\boldsymbol{x} + \boldsymbol{r}$ with distance $|\boldsymbol{r}| = r$ and time lag τ. We calculate the velocity at a particle position $\boldsymbol{x}(t)$ by $\boldsymbol{v}(\boldsymbol{x}, t) = (\boldsymbol{x}(t + \Delta t) - \boldsymbol{x}(t))$. The interval Δt between the timesteps is chosen such that, on average, each charge carrier in the system can jump once within the interval, and therefore, increases linearly with increasing V_G. We consider the entire ensemble and thus divide by the number $N(r,\ t)$ of pairwise velocities considered for the sum, and we also take the average over 50 timesteps. Since in OFETs, most charges occupy only the lowest layer [5, 42], the nature of the transport is mostly 2D, and therefore, we consider the transport in the x- and the y-direction only. For zero time lag ($\tau = 0$), the VCCF gives the spatial coherence of hopping velocities within a certain distance r and within a single time interval Δt.

Figure 8 shows this spatial coherence for the system with $\sigma =$ 5 meV, $T = 100$ K, and different gate voltages. $C_{xx}(r, \tau = 0)$ gives the spatial coherence in the x-direction, i.e., parallel to the direction of the source-drain field, while $C_{yy}(r, \tau = 0)$ measures spatial coherences perpendicular to the applied field direction. For large distances, e.g., $r > 10$ nm, there is no correlation in direction perpendicular to the applied field between two quasi-simultaneous hops $C_{yy}(r < 10\ \text{nm},\ \tau = 0) = 0$. That is perfectly in agreement with the notion that an electric field should not impact charge transport perpendicular to it. Similarly, we find a constant velocity correlation for jumps in field direction: $C_{xx}(r < 10\ \text{nm},\ \tau = 0) = const.$ It is not surprising that two jumps are correlated, i.e., if one carrier jumps, its neighbor jumps in the same direction with a finite probability, when an external field is applied.

At shorter distances, correlations appear that are not induced by the applied field but can be attributed to the Coulomb interaction between carriers. For example, if two carriers with a separation of, say $r < 4$ nm in the case of 20 V, hop quasi-simultaneously, then $C_{yy}(r < 4\ \text{nm},\ \tau = 0) < 0$, implying that their velocities in the y-direction are opposite (Figure 8b). For two identical charges, this must be a repulsive rather than attractive motion. With a higher separation distance, C_{yy} has a small maximum, which shall be discussed below. Note that for $r < 1$ nm the velocity correlation function trivially approaches zero, as there are no pairs of charges within this distance. For $V_G = 20$ V, we also observe opposite velocity components in the direction of the electric field if two hopping carriers are closer than 3 nm. However, for larger distances, and also generally for larger gate voltages (i.e., carrier densities), C_{xx} is positive. Thus, charge pairs move in the same direction, and the jump of a charge correlates with the jump of an adjacent one. The important feature is that C_{xx} shows a maximum. In other words, at a certain distance from a jumping carrier, there is a higher probability for another carrier jumping in the same direction than further away from it. The Coulomb interaction between charges pushes a neighboring charge more strongly along the field direction than it would otherwise move. For $V_G = 20$ V, this is at $r_{max} = 4.9$ nm, and this distance decreases with gate voltage since the charge concentration increases and the distances between charges get smaller. As mentioned before, we also observed similar maxima for C_{yy}, indicating that pushes occur perpendicular to the field direction as well, although less pronounced due to the weaker correlation maxima. This is reasonable, since motion along this axis is not enhanced by the electric field. The negative minimum of C_{xx} at small distances also vanishes for higher gate voltages. We attribute this to the presence of too many neighbors moving in the field direction so that a carrier can no longer move in the opposite direction without coming too close to another carrier that moves in the field direction.

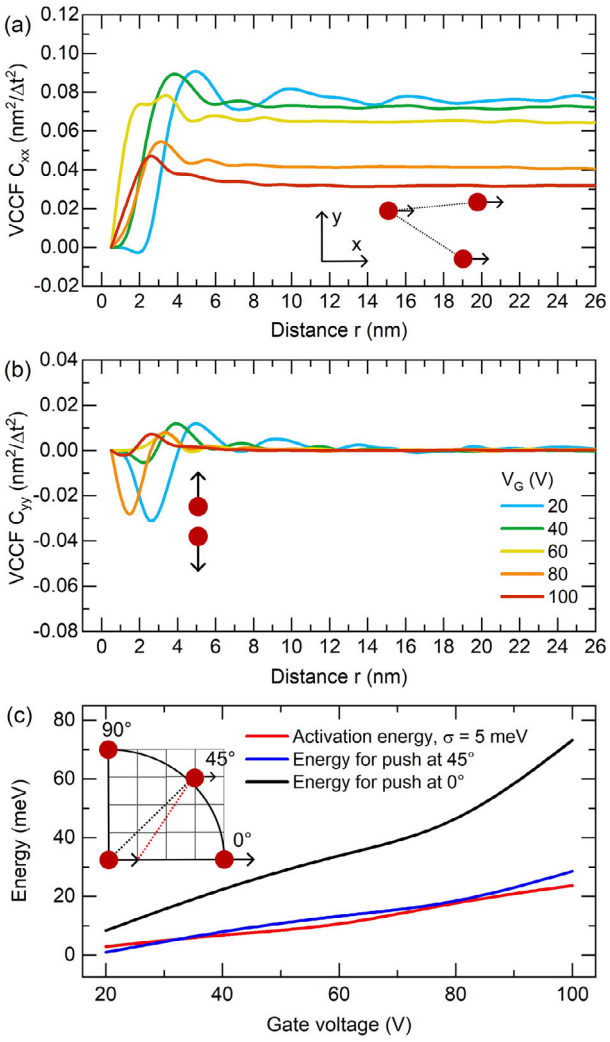

FIGURE 8 | Velocity cross-correlation (a) C_{xx} and (b) C_{yy} at zero time lag for several gate voltages at $\sigma = 5$ meV and $T = 100$ K, showing the spatial coherence within one time interval for the x- and y-components of the velocity. The time interval is chosen so that each particle can jump once on average during that time. Red circles with black arrows indicate the direction of carrier movement considered; the source-drain field is oriented in x-direction. (c) The energy required to jump in the field direction against the Coulombic field of a neighboring particle at a certain distance when the neighboring particle is approached at an angle of 45° (blue) and when it is approached frontally (black). The distance between the charges before the approach is taken as the distance at which maximal correlation is observed in (a). For comparison, the activation energy for $\sigma = 5$ meV is a red line.

The maxima in the velocity correlation function that we observe for distances between about 2 and 5 nm hence, represent the positions of a neighboring charge that is "pushed" by its neighbor.

In the following, we aim to provide a rough estimate of the energy E_{push} required to push a charge at a distance r_{max}. For a charge to push its neighbor, it needs to approach and, to do so, must have the energy to overcome the potential difference created by the field of its neighbor.

Consider a charge that moves around 1 nm in the field direction, thus approaching another charge. We neglect energetic disorder. Depending on the angle of approach, the distance between the two charges will change. The potential barrier E_{push} for the approaching charge in the field of the other is given by the difference in Coulomb potential at r_{max} after the jump, minus the field contribution of 0.01 eV/nm. Figure 8c shows E_{push} for an angle of 0° as a black line, assuming a direct approach, and for 45° (the average angle under which an approach can occur), as a blue line. For comparison, the activation energy for the $\sigma = 5$ meV system (from Figure 4) is shown as a red line. It is remarkable how well the activation energy matches E_{push} under 45°. Both potential curves exhibit a monotonic increase with the gate voltage, with a similar slope, and their absolute values differ by only a few meV. While the forward approach under 45° between two charges seems realistic, approaches between two charges under 0° are unlikely to happen, as the required energy mostly exceeds thermal energy at room temperature. The values we derived by this estimate for a forward approach under 45° are also consistent with the average energy barrier we found when averaging over hops with a positive transition energy (Figure 7). Even though the measured activation energy agrees well with our estimate for E_{push}, we caution that this is a rough approximation. Not all charges will hop in the field direction, nor over the estimated distance, nor directly along the field gradient of one single other charge. Rather, they move in the field of many more neighbors, which also arrange themselves energetically in the most favorable way possible.

In summary, we have shown, for a nearly disorder-free system, that charges move in their own potential minimum, which is created by the Coulomb repulsion to other charges. Additionally, we find that at a certain distance, hopping directions of neighboring charges are correlated. Also at that distance, the energy for one charge to approach another under a 45° angle agrees reasonably well with the determined activation energy (c.f. Figure 8c). Furthermore, on average, yet not always, charges hop "in fair weather" [30], i.e., when they are off-centered in their potential minimum through a rearrangement of the other charges. Hence, average hops proceed sequentially, with virtually no thermal activation (cf. Figure 6), while occasionally, hops require activation energy, which then becomes rate-limiting. This is consistent with the case in a Coulomb glass [27, 31].

With this, we propose a new interpretation of activation energy that extends the picture we are familiar with for low and medium charge carrier densities, where carrier-carrier interactions are negligible. There, the activation energy elevates charges to the transport level, where they can move more easily, as there are many free sites of similar energy and hops between them require small or no thermal activation. In contrast, at high charge carrier concentrations, the average hopping event also requires small or no thermal activation, as it occurs when the potential cloud around the charge carrier has rearranged, making the hop energetically favorable. This correlation-driven transport is analogous to the effortless movements at the transport level. However, not all hops are energetically favorable or with only a small barrier: We observe that some charges push each other with an energy of the same order of magnitude as the activation energy. Analogous to the classical activation energy that is necessary to bring a charge to the transport level once in a while, these occasional pushes seem to be necessary to enable energetically favorable transport the rest of the time. The activation energy is therefore responsible for the spatial rearrangement of charges, when most of them are already in their energetically favorable position and would not move otherwise.

3 | Discussion

The present formalism for charge transport in an organic semiconductor with a high charge carrier concentration appears to be characteristic of that of a Coulomb glass. The classic concept that Efros and Shklovskii developed [24] is based on Mott's variable range hopping (VRH) concept [54] and shows that, under consideration of Coulomb interactions between charges, a gap between full and empty states in the DOS develops. Importantly, in the classical concept, the interaction for the hopping of the charge can be long-ranged, i.e., the localization length is a multiple of the inter-site separation. This is realized in inorganic semiconductors. The Efros-Shklovskii (ES) $\mu(T) \propto \exp\left(-(T_0/T)^{\frac{1}{2}}\right)$ dependence relates the charge carrier mobility and temperature. The characteristic temperature T_0 corresponds to a localization length $\xi = \frac{Ce^2}{\varepsilon_0 \varepsilon_r k_B T_0}$ for 2D (3D) transport [25], with the numerical coefficient $C_{2D} = 6.2$ [55] ($C_{3D} = 2.8$ [25]). This relationship has been verified for inorganic semiconductors, and T_0 was found to be at very low to low temperatures, yielding localization lengths on the order of 10^3 nm [56, 57]. Analyzing the temperature dependence of the mobility in an organic hopping system at high charge concentration (c.f. Figure 4) in terms of $\mu(T) \propto \exp\left(-(T_0/T)^{\frac{1}{2}}\right)$, we end up with a characteristic temperature $T_0 = 2012$ K. This value is one to two orders of magnitude higher than for inorganic semiconductors [56, 57], since the Coulomb gap in organic semiconductors is established at ambient temperature, but the ratio T_0/T is comparable. The characteristic temperature would correspond to a localization length of $\xi_{2D} = 162$ nm ($\xi_{3D} = 73$ nm). This is much larger than the localization length we used in our simulations ($\gamma^{-1} = 0.2$ nm), which is characteristic of organic semiconductors, and larger than the model dimensions. Evidently, an organic Coulomb glass resembles the behavior of an inorganic system, but parametrically, it is quite different from an inorganic system [25, 56, 57].

We also recall that in our model, the maximum hopping radius was $r_{max} = \sqrt{3}$ nm since charge transport in organic materials occurs via mostly nearest jumps [27]. Thus, our model does not include VRH, yet we still observe a Coulomb gap and Coulomb glass behavior. This proves that the formation of a Coulomb glass does not necessarily require the variable-range-hopping concept. With VRH, even though charge transfer to distant sites is technically allowed, charges should only move to sites in their vicinity, as all other sites are energetically unfavorable due to Coulomb repulsion from other charges (c.f. Figure 6). Thus,

in combination with Coulomb repulsion, the VRH imposes a similar restriction on the system as our model does with a small maximum hopping radius. In both cases, the charges are strongly localized and can not hop to distant sites. In this respect, the emergence of the Coulomb gap in organic semiconductors is not surprising. Here, the electronic states are strongly localized and follow an already disordered distribution similar to a Coulomb glass, even at low carrier densities.

The DOS with its Coulomb gap is a quantity that is not always straightforward to access, so one may ask how the dominance of Coulomb interactions may be identified in the charge transport characteristics. One clear indicator of a strongly pronounced (hard) Coulomb gap is the observation of an ES temperature dependence. However, in our data, we observe the emergence of a (soft) Coulomb gap even at room temperatures and high disorders such as $\sigma = 75$ meV, where the temperature dependence is still Arrhenius-like. As mentioned in the context of Figure 4, the increase in activation energy with gate voltage, respectively carrier density, is also a clear indicator for the emergence of a fundamentally different transport regime, so that the minimum of the activation energy may serve as an indicator for a transition from a disorder-controlled transport regime to one dominated by the Coulomb gap.

How can charge carrier densities that sustain a Coulomb gap be achieved? As evident in Equation (4), high charge carrier densities require a thin insulator, a high permittivity, and a high gate voltage while maintaining a high resistance to dielectric breakdown. Note, however, that the use of a very high permittivity material, which would allow for higher insulator thicknesses and lower gate voltages, can lead to additional polaronic effects as demonstrated by Fratini et al. and related work [11, 53]. If we take the minimum of the concentration-dependent activation energy as a signature for the onset of dominant Coulomb interactions, we would expect to see dominant Coulomb effects for a sample with an energetic disorder of $\sigma = 75$ meV and a dielectric constant of $\varepsilon_r = 4$, and otherwise similar parameters to our system, from at about $V_G = 50$ V onward, provided the sample can sustain that voltage without dielectric breakdown. This corresponds to about 10^{13} cm^{-2} (10% charges per site in the lowest layer).

A high charge carrier density can be achieved more easily in EGOFETs and OECTs than in OFET structures, yet counter-ions play a crucial role in these systems and complicate the description of charge transport, so that it is not clear a priori whether a Coulomb gap can be observed in these systems. The difficulties associated with the description of Coulomb interaction in electrochemically doped systems are the reason why, in this study, we chose to focus on the simple case of transport in a non-doped OFET system. Nevertheless, future work should certainly address the question of whether a Coulomb gap may also emerge in systems where high carrier densities can be achieved easily by electrochemical doping.

Our KMC approach can only be a first step in the exploration of the charge carrier dynamics in organic Coulomb glasses. It has several limitations; for example, the dielectric permittivity is assumed to be spatially uniform and independent of carrier density. The extent to which this actually holds and a carrier density-dependent permittivity may modify the charge carrier dynamics needs to be addressed in future work. Similarly, our KMC approach approximates the quasi-collective motion of the carrier ensemble by a sequence of correlated single carrier hops. However, in principle, once the carrier motion approaches a collective behavior, the consideration of true multi-particle hopping rates would be appropriate. Clearly, the calculation of all possible multi-particle transition rates for the entire ensemble to any possible next configuration is challenging and beyond the scope of this work. Our approach effectively approximates the multi-particle transition process by a sequence of single-particle transitions. The fact that our simulations converge is a first indication that this approach may be reasonable. Moreover, it is justified by the fact that we consider at most 22% site occupancy. Future work may wish to consider how this needs to be modified for higher charge carrier densities. Similarly, future work might consider how the threshold for the onset of dominant Coulomb effects changes when the DOS is a priori asymmetric. This can occur, for example, when the molecular interactions are strong, and bands begin to form—the DOS tends toward a square root shape that is very broad and asymmetric.

Finally, we studied cases of very low disorder, where the assumption of localization is only justified when the coupling between sites is weaker than the prevailing disorder. This is the case, for example, where side chains effectively screen π-interactions. For molecular crystals made from molecules without large side chains, this may not necessarily be the case. Addressing the extent to which stronger intermolecular coupling and the emergence of bands modify the picture outlined in this work will also be a worthwhile topic for future studies.

4 | Conclusion

We studied the dependence of charge transport on the charge carrier density for a non-doped organic semiconductor (without counter-ions) by means of Kinetic Monte-Carlo simulations, and we observed a continuous, yet fundamental change in the nature of this transport. While at low charge concentrations, transport can be described by considering merely a single carrier that hops from the Fermi level to the transport level via thermal activation, at high carrier densities, hopping becomes Coulomb-correlated so that the entire ensemble of charges needs to be considered. The charges no longer hop from the Fermi level to the transport level but rather from slightly below the center of the ODOS, with the activation energy bringing them to that center. The activation energy is the energy needed to accomplish the structural reorganization of charges in the ensemble so that charge transport can proceed.

In agreement with previous studies [15, 33, 34], we find an energy gap between the distribution of unoccupied and occupied sites (Coulomb gap) that emerges as a consequence of the Coulomb interaction between charges. Comparison to inorganic semiconductors demonstrates that the appearance of a Coulomb gap does not require long-range hops (as needed in the variable-range hopping model by Mott) nor low temperatures. It suffices if charge carriers are spatially localized yet subject to long-range Coulomb interactions. We consider that our work indicates a transport regime that has hardly been explored so far in organic semiconductors.

Acknowledgements

We thank Andriy Kadashchuk for helpful discussions and Tobias Meier for preliminary studies. A.K. and H.O. acknowledge financial support from the Bavarian State Ministry for Science and Arts through the initiative "Solar Technologies go Hybrid (SolTech)" and the German Science Foundation (DFG) for funding within project number 492 723 217 (CRC 1585 MultiTrans, projects B01 and B04). H.B. thanks the Bayreuth Institute for Macromolecular Research (BIMF) for support. M.S.D. was supported by the elite network of Bavaria (Study Program Biological Physics) and the University of Bayreuth Graduate School. Calculations were performed using the Emil cluster of the Bayreuth Centre for High Performance Computing (https://www.bzhpc.uni-bayreuth.de), funded by the Deutsche Forschungsgemeinschaft (DFG, German Research Foundation) – 422127126.

Open access funding enabled and organized by Projekt DEAL.

Conflicts of Interest

The authors declare no conflicts of interest.

Data Availability Statement

The data that support the findings of this study are available from the corresponding author upon reasonable request.

References

1. L. Xiang, W. Wang, and W. Xie, "Achieving High Mobility, Low-Voltage Operating Organic Field-Effect Transistor Nonvolatile Memory by an Ultraviolet-Ozone Treating Ferroelectric Terpolymer," *Scientific Reports* 6 (2016): 36291, https://doi.org/10.1038/srep36291.

2. S. H. Rhee, K. B. Nam, C. S. Kim, et al., "Effect of Electron Mobility of the Electron Transport Layer on Fluorescent Organic Light-Emitting Diodes," *ECS Solid State Letters* 3 (2014): R19–R22.

3. C. Wang, R. C. I. MacKenzie, U. Würfel, et al., "Transport Resistance Dominates the Fill Factor Losses in Record Organic Solar Cells," *Advanced Energy Materials* 16 (2025): 2405889.

4. B. Amna and T. Ozturk, "Organic Field-Effect Transistor-Based Sensors: Recent Progress, Challenges and Future Outlook," *Journal of Materials Chemistry C* 13 (2025): 8354–8424, https://doi.org/10.1039/D4TC04265D.

5. M. Mottaghi and G. Horowitz, "Field-Induced Mobility Degradation in Pentacene Thin-Film Transistors," *Organic Electronics* 7 (2006): 528–536, https://doi.org/10.1016/j.orgel.2006.07.011.

6. Y. Xia, W. Xie, P. P. Ruden, and C. D. Frisbie, "Carrier Localization on Surfaces of Organic Semiconductors Gated with Electrolytes," *Physical Review Letters* 105 (2010): 036802, https://doi.org/10.1103/PhysRevLett.105.036802.

7. I. Vladimirov, S. Müller, R.-P. Baumann, et al., "Dielectric–Semiconductor Interface Limits Charge Carrier Motion at Elevated Temperatures and Large Carrier Densities in a High-Mobility Organic Semiconductor," *Advanced Functional Materials* 29 (2019): 1807867, https://doi.org/10.1002/adfm.201807867.

8. S. Jiang, J. Qian, Q. Wang, et al., "Probing Coulomb Interactions on Charge Transport in Few-Layer Organic Crystalline Semiconductors by the Gated van der Pauw Method," *Advanced Electronic Materials* 6 (2020): 2000136, https://doi.org/10.1002/aelm.202000136.

9. W. Choi, W. Matsuda, and S. Seki, "Impact of Gate Voltage on Mobility of Charge Carriers in Conductive Channel of Organic Molecular Semiconductors: Transport Landscape Assessed by Alternating and Direct Current Mode Techniques," *Advanced Electronic Materials* 11 (2025): 2400304, https://doi.org/10.1002/aelm.202400304.

10. A. Köhler and H. Bässler, *Electronic Processes in Organic Semiconductors: An Introduction* (Wiley-VCH Verlag GmbH & Co. KGaA, Weinheim, 2015).

11. S. Fratini, H. Xie, I. N. Hulea, S. Ciuchi, and A. F. Morpurgo, "Current Saturation and Coulomb Interactions in Organic Single-Crystal Transistors," *New Journal of Physics* 10 (2008): 033031, https://doi.org/10.1088/1367-2630/10/3/033031.

12. T. Uemura, C. Rolin, T. Ke, et al., "On the Extraction of Charge Carrier Mobility in High-Mobility Organic Transistors," *Advanced Materials* 28 (2016): 151–155, https://doi.org/10.1002/adma.201503133.

13. C. Rolin, E. Kang, J.-H. Lee, G. Borghs, P. Heremans, and J. Genoe, "Charge Carrier Mobility in Thin Films of Organic Semiconductors by the Gated van der Pauw Method," *Nature Communications* 8 (2017): 14975, https://doi.org/10.1038/ncomms14975.

14. J. Zhou, Y. C. Zhou, J. M. Zhao, C. Q. Wu, X. M. Ding, and X. Y. Hou, "Carrier Density Dependence of Mobility in Organic Solids: a Monte Carlo Simulation," *Physical Review B* 75 (2007): 153201, https://doi.org/10.1103/PhysRevB.75.153201.

15. M. Koopmans, M. A. T. Leiviskä, J. Liu, et al., "Electrical Conductivity of Doped Organic Semiconductors Limited by Carrier–Carrier Interactions," *ACS Applied Materials & Interfaces* 12 (2020): 56222–56230, https://doi.org/10.1021/acsami.0c15490.

16. F. Liu, H. van Eersel, B. Xu, et al., "Effect of Coulomb Correlation on Charge Transport in Disordered Organic Semiconductors," *Physical Review B* 96 (2017): 205203, https://doi.org/10.1103/PhysRevB.96.205203.

17. J. J. M. van der Holst, F. W. A. van Oost, R. Coehoorn, and P. A. Bobbert, "Monte Carlo Study of Charge Transport in Organic Sandwich-Type Single-Carrier Devices: Effects of Coulomb Interactions," *Physical Review B* 83 (2011): 085206, https://doi.org/10.1103/PhysRevB.83.085206.

18. A. Sharma, F. W. A. van Oost, M. Kemerink, and P. A. Bobbert, "Dimensionality of Charge Transport in Organic Field-Effect Transistors," *Physical Review B* 85 (2012): 235302, https://doi.org/10.1103/PhysRevB.85.235302.

19. X. Yang, G. Ye, J. Liu, R. C. Chiechi, and L. J. A. Koster, "Carrier–Carrier Repulsion Limits the Conductivity of N-Doped Organic Semiconductors," *Advanced Materials* 36 (2024): 2404397, https://doi.org/10.1002/adma.202404397.

20. J. Liu, M. P. Garman, J. Dong, et al., "Doping Engineering Enables Highly Conductive and Thermally Stable n-Type Organic Thermoelectrics with High Power Factor," *ACS Applied Energy Materials* 2 (2019): 6664–6671, https://doi.org/10.1021/acsaem.9b01179.

21. J. Liu, L. Qiu, G. Portale, et al., "Side-Chain Effects on N-type Organic Thermoelectrics: a Case Study of Fullerene Derivatives," *Nano Energy* 52 (2018): 183–191, https://doi.org/10.1016/j.nanoen.2018.07.056.

22. C. D. Frisbie, "Crossing the Coulomb Gap in Semiconducting Polymers," *Nature Materials* 23 (2024): 1615–1617, https://doi.org/10.1038/s41563-024-01965-2.

23. D. H. L. Tjhe, X. Ren, I. E. Jacobs, et al., "Non-Equilibrium Transport in Polymer Mixed Ionic–Electronic Conductors at Ultrahigh Charge Densities," *Nature Materials* 23 (2024): 1712–1719, https://doi.org/10.1038/s41563-024-01953-6.

24. A. L. Efros and B. I. Shklovskii, "Coulomb Gap and Low Temperature Conductivity of Disordered Systems," *Journal of Physics C: Solid State Physics* 8 (1975): L49–L51, https://doi.org/10.1088/0022-3719/8/4/003.

25. B. I. Shklovskii and A. L. Efros, *Electronic Properties of Doped Semiconductors* (Springer Berlin, Heidelberg, 1984).

26. A. L. Efros, "Coulomb Gap in Disordered Systems," *Journal of Physics C: Solid State Physics* 9 (1976): 2021–2030, https://doi.org/10.1088/0022-3719/9/11/012.

27. J. H. Davies, P. A. Lee, and T. M. Rice, "Properties of the Electron Glass," *Physical Review B* 29 (1984): 4260–4271, https://doi.org/10.1103/PhysRevB.29.4260.

28. A. Möbius, M. Richter, and B. Drittler, "Coulomb Gap in Two-and Three-Dimensional Systems: Simulation Results for Large Samples," *Physical Review B* 45 (1992): 11568.

29. E. R. Grannan and C. C. Yu, "Critical Behavior of the Coulomb Glass," *Physical Review Letters* 71 (1993): 3335–3338, https://doi.org/10.1103/PhysRevLett.71.3335.

30. A. L. Efros, "Coulomb Gap and Transport in Classical Electron Liquid," *Physical Review Letters* 68 (1992): 2208–2211, https://doi.org/10.1103/PhysRevLett.68.2208.

31. J. Bergli, A. M. Somoza, and M. Ortuño, "Effects of Many-Electron Jumps in the Relaxation and Conductivity of Coulomb Glasses," *Physical Review B* 84 (2011): 174201, https://doi.org/10.1103/PhysRevB.84.174201.

32. B. I. Shklovskii, "Half-Century of Efros–Shklovskii Coulomb Gap: Romance with Coulomb Interaction and Disorder," *Low Temperature Physics* 50 (2024): 1101–1112.

33. S. Ihnatsenka, "Model of the Thermoelectric Properties of Anisotropic Organic Semiconductors," *ACS Physical Chemistry Au* 2 (2022): 118–124, https://doi.org/10.1021/acsphyschemau.1c00031.

34. F. Liu, Y. Su, X. Lin, et al., "Image-Force-Stabilized Interfacial Dipole Layer Impedes Charge Injection into Disordered Organic Semiconductors," *Physical Review Applied* 17 (2022): 024003, https://doi.org/10.1103/PhysRevApplied.17.024003.

35. Y. N. Gartstein and E. M. Conwell, "High-Field Hopping Mobility in Molecular Systems with Spatially Correlated Energetic Disorder," *Chemical Physics Letters* 245 (1995): 351–358, https://doi.org/10.1016/0009-2614(95)01031-4.

36. S. L. M. van Mensfoort, V. Shabro, R. J. de Vries, R. A. J. Janssen, and R. Coehoorn, "Hole Transport in the Organic Small Molecule Material α-NPD: Evidence for the Presence of Correlated Disorder," *Journal of Applied Physics* 107 (2010): 113710, https://doi.org/10.1063/1.3407561.

37. H. Bässler, "Localized States and Electronic Transport in Single Component Organic Solids with Diagonal Disorder," *physica status solidi* 107 (1981): 9–54.

38. H. Bässler, "Charge Transport in Disordered Organic Photoconductors. A Monte Carlo Simulation Study," *physica status solidi* 175 (1993): 15.

39. V. I. Arkhipov, E. V. Emelianova, and G. J. Adriaenssens, "Effective Transport Energy versus the Energy of Most Probable Jumps in Disordered Hopping Systems," *Physical Review B* 64 (2001): 125125, https://doi.org/10.1103/PhysRevB.64.125125.

40. S. D. Baranovskii, "Theoretical Description of Charge Transport in Disordered Organic Semiconductors," *physica status solidi* 251 (2014): 487.

41. A. V. Nenashev, J. O. Oelerich, and S. D. Baranovskii, "Theoretical Tools for the Description of Charge Transport in Disordered Organic Semiconductors," *Journal of Physics-Condensed Matter* 27 (2015): 093201.

42. H. Li, Y. Li, H. Li, and J.-L. Brédas, "Organic Field-Effect Transistors: a 3D Kinetic Monte Carlo Simulation of the Current Characteristics in Micrometer-Sized Devices," *Advanced Functional Materials* 27 (2017): 1605715, https://doi.org/10.1002/adfm.201605715.

43. I. I. Fishchuk, D. Hertel, H. Bässler, and A. K. Kadashchuk, "Effective-Medium Theory of Hopping Charge-Carrier Transport in Weakly Disordered Organic Solids," *Physical Review B* 65 (2002): 125201, https://doi.org/10.1103/PhysRevB.65.125201.

44. M. S. Dörfler, H. Bässler, A. Kadashchuk, H. Oberhofer, and A. Köhler, "Identifying Pitfalls When Using the Miller–Abrahams Rate in Kinetic Monte Carlo Simulations," *Journal of Materials Chemistry C* 13 (2025): 14962–14971.

45. A. Miller and E. Abrahams, "Impurity Conduction at Low Concentrations," *Physical Review* 120 (1960): 745–755, https://doi.org/10.1103/PhysRev.120.745.

46. R. P. Fornari, J. Aragó, and A. Troisi, "A Very General Rate Expression for Charge Hopping in Semiconducting Polymers," *The Journal of Chemical Physics* 142 (2015): 184105, https://doi.org/10.1063/1.4920945.

47. V. Coropceanu, J. Cornil, D. A. Da Silva Filho, Y. Olivier, R. Silbey, and J.-L. Brédas, "Charge Transport in Organic Semiconductors," *Chemical Reviews* 107 (2007): 926–952, https://doi.org/10.1021/cr050140x.

48. J. Bardeen and W. Shockley, "Deformation Potentials and Mobilities in Non-Polar Crystals," *Physical Review* 80 (1950): 72–80, https://doi.org/10.1103/PhysRev.80.72.

49. H. Li and J.-L. Brédas, "Developing Molecular-Level Models for Organic Field-Effect Transistors," *National Science Review* 8 (2020): nwaa167.

50. H. Li and J.-L. Brédas, "Kinetic Monte Carlo Modeling of Charge Carriers in Organic Electronic Devices: Suppression of the Self-Interaction Error," *The Journal of Physical Chemistry Letters* 8 (2017): 2507–2512, https://doi.org/10.1021/acs.jpclett.7b01161.

51. N. Metropolis, A. W. Rosenbluth, M. N. Rosenbluth, A. H. Teller, and E. Teller, "Equation of State Calculations by Fast Computing Machines," *The Journal of Chemical Physics* 21 (1953): 1087–1092, https://doi.org/10.1063/1.1699114.

52. A. Y. Toukmaji and J. A. Board, "Ewald Summation Techniques in Perspective: a Survey," *Computer Physics Communications* 95 (1996): 73–92, https://doi.org/10.1016/0010-4655(96)00016-1.

53. I. N. Hulea, S. Fratini, H. Xie, et al., "Tunable Fröhlich Polarons in Organic Single-Crystal Transistors," *Nature Materials* 5 (2006): 982–986, https://doi.org/10.1038/nmat1774.

54. N. F. Mott, "Conduction in Glasses Containing Transition Metal Ions," *Journal of Non-Crystalline Solids* 1 (1968): 1–17, https://doi.org/10.1016/0022-3093(68)90002-1.

55. V. L. Nguyen, *Fizika i Tekhnika Poluprovodnikov* 18 (1984): 335.

56. K. M. Itoh, E. E. Haller, J. W. Beeman, et al., "Hopping Conduction and Metal-Insulator Transition in Isotopically Enriched Neutron-Transmutation-Doped 70 Ge:Ga," *Physical Review Letters* 77 (1996): 4058–4061, https://doi.org/10.1103/PhysRevLett.77.4058.

57. J. Zhang, W. Cui, M. Juda, et al., "Hopping Conduction in Partially Compensated Doped Silicon," *Physical Review B* 48 (1993): 2312–2319, https://doi.org/10.1103/PhysRevB.48.2312.

Supporting Information

Additional supporting information can be found online in the Supporting Information section.

Supporting File: adma72828-sup-0001-SuppMat.docx.